



Research Article

Mixed convective flow of heat and mass transfer of nanofluids over a static wedge with convective boundary conditions

M. Sreedhar BABU¹, V. Venkata RAMANA¹, G. Ravi SHANKAR¹, C.S.K. RAJU^{2,*}

¹Department of Applied Mathematics, Y.V. University, Kadapa, A.P., India

²Department of Mathematics, GITAM School of Science, GITAM University, Bengaluru-Campus, Karnataka-562163, India

ARTICLE INFO

Article history

Received: 03 February 2020

Accepted: 22 July 2020

Key words:

Nanofluid; Wedge surface;
Mixed convection; Convective
heat and mass conditions

ABSTRACT

With the fast improvement of the industry and the utilization of inventive strategies, scientists want to think over the steady blending convection of water-based nanofluids past static wedges. The Buongiorno model with convection is applied. Also, incorporated the Brownian motion and thermophoresis. The attention is on the nature of mixed wedge-formed convective heat and mass transfer of the nanofluid flow. Utilizing comparable change, the governing partial differential equations (PDEs) are reduced to ordinary differential equations (ODEs) solved by the R-K Gill method. The physical quantities of velocity, temperature and concentration fields, as well as diffusion and thermal transfer rates with friction factor coefficients, is discussed. The investigation demonstrated that the temperature convergence of the liquid was higher within the sight of the thermophoresis parameter and Biot numbers. It has been seen that divider pressure increments with expanding wedge and mixed convection parameters.

Cite this article as: Babu MS, Ramana VV, Shankar GR, Raju CSK. Mixed convective flow of heat and mass transfer of nanofluids over a static wedge with convective boundary conditions. J Ther Eng 2021;7(Supp 14):1958–1969.

INTRODUCTION

The most popular inquiry concerning traditional liquid elements is the laminar stream on a fixed surface. At the point when the free current gives off an impression of being parallel to the surface and the liquid speed seems consistent, then the “Blasius issue” happens. In any case, when the surface is at an edge to the free current, the issue is known as a “wedge stream issue”. As of late, because of the wide use of liquid stream on wedge-formed surfaces in geothermal frameworks, unrefined petroleum extraction, streamlined

features, heat exchangers, polymer handling, and design preparation, scientists have pulled in broad consideration Science, atomic waste stockpiling, and so on. Falkner and Skan made an authoritative showing around there [1]. They envisaged wedge issues by considering incompressible thick two-dimensional liquid stream. They applied a closeness change strategy that improved the nonlinear fractional differential conditions into conventional differential conditions. Afterward, Hartree [2] significantly extended the outcomes made by Falkner and Skan [1], utilizing $f''(0)$ as a free

*Corresponding author.

*E-mail address: rchakrav@gitam.edu

This paper was recommended for publication in revised form by
Regional Editor Pouria Ahmadi



parameter. In outline, the parameter of the wedge point has been taken as $\beta\pi$, where $\beta > 0$ demonstrates that the current is near the wedge and $\beta < 0$ shows the backward. Then again, $\beta = 0$ is identified with the Blasius flow, which is the situation for even plates. Stewartson [3] and Hastings [4] demonstrated that under the state of $0.0 \leq \beta \leq 1.0$, Falkner condition can be gotten. They show that when $-0.1988 \leq \beta \leq 0.0$, two stages can be gotten: one is $f''(0) > 0$ and the other is $f''(0) < 0.0$. All things considered, it very well may be found in the article by Botta et al. [5] for $x < 0$, when $\beta > 1.0$, the readiness of Falkner and Skan conditions is self-evident. By including all these parameters considered, it very well may be found in the article by Botta et al. [5] for $0.0 < f''(0) < 1$, when $\beta > 1.0$, the plan of Falkner and Skan condition is self-evident. Yih [6] examined the constrained progression of a wedge-formed convective boundary layer by applying suction and infusion powers. Another time, Watanabe [7] explored the progression of the boundary layer through the wedge within the sight of suction and infusion. Rajagopal [8] utilized auxiliary liquid to examine the wedge issue. Zaturka and Banks attempted another inventive strategy to take care of the Falkner and Skan issue [9]. They found an answer to the parameter β work. Na [10] presented a lot of changes and afterward changed the Falkner condition into a few introductory worth issues with the assistance of immediate incorporation conspire. Asaithambi [11] utilizes a boundary distinction plan to tackle the Falkner and Skan conditions.

Logical advancement is a broadly existing reality that influences all parts of the fast improvement of industrialization in this day and age. For clear reasons, from vitality preservation, it is essential to make propelled enhancements to warm move innovation. Ordinary warmth move liquids, for example, water, lamp fuel, ethylene glycol, have lower warm conductivity, yet resulting exploration and examinations have prompted the advancement of nanofluidic frames in which nano-sized particles are added to the base liquid to expand boundary. Heat moves of base liquid. New research on the Boundary layer stream of nanofluids keeps on pulling in expanding enthusiasm because of its wide and assorted applications. Yacob et al, they covered Falkner and Skan's inquiry concerning static or moving wedges assimilated in nanofluids [12]. Chamkha et al. [13] the impact of radiation on consolidated convection were inspected in an isothermal vertical wedge in a porous medium loaded up with nanofluids. Gorla et al. [14] reported blended convection through a vertical wedge, which is drenched in a permeable medium with nanofluids. Khan and Pop [15] contemplated the progression of nanofluids over moving wedges. Likewise, Kasamani et al. [16] researched the progression of nanofluids on wedges within the sight of suction/infusion. Research by Kandasamy et al. [17] adds new viewpoints to these examinations. The utilization of sun based radiation to examine the progression of Hemingz from copper-water nanofluids on permeable wedges. Das

et al. [18] report the variable properties of liquids in nanofluid streams on wedges within the sight of surface slip. Gangadhar et al. [19] examined the insecure progression of free convective boundary layers of nanofluids on extended surfaces. Gangadhar et al. [20] considered the impact of warm radiation on the progression of nanofluids from oil through penetrable wedges.

The investigation of liquid stream in stagnation zones has its very own significance in the fields of designing and applied sciences. At the point when liquids stagnate symmetrically on a strong divider, Hiemenz [21] talks about the progression of viscous liquids. Stuart [22] inspected stream examination with uniform vortices because of stagnation focuses. Chiam [23] and Wang [24] inspected the progression of stagnation directs nearby toward the stretch/shrivel edge, separately. Frossling [25] and Homann [26] dissected the pivotal even progression of Newtonian liquid close to the stagnation point. Howarth [27] and Davey [28] considered three-dimensional flows up to the stagnation point. Labropulu et al. [29] analyzed the impact of unsteadiness parameters on the helper liquid stream to the stagnation point. Sandeep et al. [30] researched the impacts of synthetic responses and prompted attractive fields in Jeffrey's nanofluid in the stagnation point stream [30] Recently, the authors [38–41] Considered the progression of heat transfer in various kind of situation such as stagnation point in a Jeffrey liquid on a greased up surface, vertical flat plate, louvered strip by using Graphene-based nanofluids etc and found it is significant in manufacturing and industrial systems.

Driven by past research, this paper tries to address the impacts of convective heat and mass conditions in wedge-formed streams inserted in nanofluids. The stream examination is performed by a comparative change that diminishes the administration condition to a standard differential condition and is fathomed utilizing the R-K Gill technique with a trigger rule. Draw some intriguing physical parameter maps for temperature and fixation fields. The physical amounts of intrigue, to be specific the neighborhood new coefficients for Skin and the nearby numbers for Nusselt and Sherwood, are determined numerically. This outcome is contrasted and related outcomes in the current writing and is palatable.

PROBLEM FORMATION AND ANALYSIS

Numerical examinations have been performed to think about the attributes of consistently blended convection on static strong wedges in free flows streaming in water-based nanofluids. The physical model and organized framework are appearing in Figure 1:

Think about a streamlined casing (x, y) along with a square shape, where the x-axis follows the heading of the current and the inside and is inverse the wedge-formed surface. At the most elevated purpose of the wedge, the

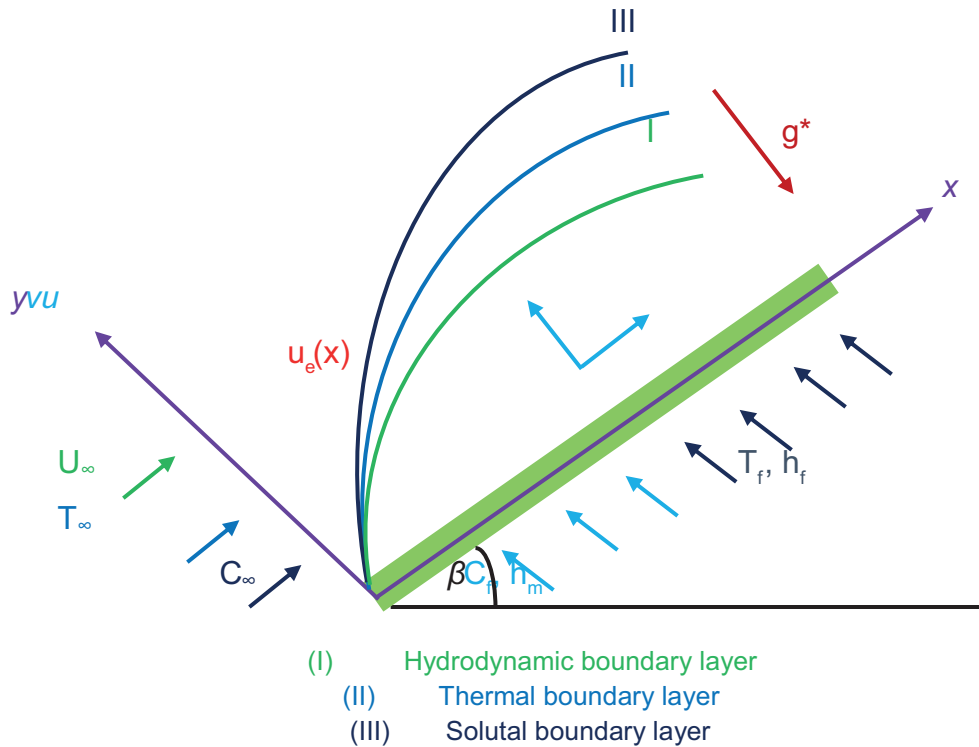


Figure 1. Physical model of the problem.

chilly fluid flood at a particular temperature T_∞ moves at a non-uniform speed $u_e(x) = U_\infty x^m$. Regardless, the hot fluid stream at temperature T_f will create a variable heat transfer coefficient (Temperature) move $h_f(x) = h_f x^{(m-1)/2}$, so it will heat the wedge-formed base surface.

Considering the presumption that the fixation at the base of the wedge is more noteworthy than C_w superficially and the free-stream focus C_∞ . Hence, the mass exchange coefficient is variable mass transfer coefficient (concentration) $h_{mass}(x) = h_{mass} x^{(m-1)/2}$ is generated. Every single warm trademark is thought to be uniform. Because of relative examination and degreasing boundary layer estimate, the scientific model of Buongiorno nanofluid moving through a wedge can be communicated as (Gorla et al. [14] and Yacob et al. [37]).

$$\frac{\partial u}{\partial x} + \frac{\partial v}{\partial y} = 0 \tag{1}$$

$$u \frac{\partial u}{\partial x} + v \frac{\partial u}{\partial y} = u_e \frac{\partial u_e}{\partial t} + u_e \frac{\partial u_e}{\partial x} + v_f \frac{\partial^2 u}{\partial y^2} + g^* \beta_T (T - T_\infty) + g^* \beta_c (C - C_\infty) \tag{2}$$

$$u \frac{\partial T}{\partial x} + v \frac{\partial T}{\partial y} = \alpha_m \frac{\partial^2 T}{\partial y^2} + \tau \left[D_B \frac{\partial C}{\partial y} \frac{\partial T}{\partial y} + \frac{D_T}{T_\infty} \left(\frac{\partial T}{\partial y} \right)^2 \right] \tag{3}$$

$$u \frac{\partial C}{\partial x} + v \frac{\partial C}{\partial y} = D_B \frac{\partial^2 C}{\partial y^2} + \frac{D_T}{T_\infty} \frac{\partial^2 T}{\partial y^2} \tag{4}$$

In this manner, the convection profile conditions utilizing the Buongiorno model superficially and away from the wedge can be composed as;

$$y = 0 : u = 0, v = 0, k_f \frac{\partial T}{\partial y} = h_f(x)(T_f - T), D_B \frac{\partial C}{\partial y} = h_{mass}(x)(C_f - C) \tag{5}$$

$$y \rightarrow \infty : u \rightarrow u_e(x) = U_\infty x^m, T \rightarrow T_\infty, C \rightarrow C \tag{6}$$

Where u and v are speed parts along the x and y axes, separately, T_f – the temperature of the liquid in the boundary layer, T_∞ – the temperature of the free current, ρ_f – thickness of the liquid, c_p – particular heat, μ – dynamic consistency, and C_∞ – free Flow fixation, D_B – Brown dissemination coefficient, D_T – heat swimming dispersion coefficient, k_f – heat conductivity coefficient, $\tau = \frac{(\rho c)_p}{(\rho c)_f}$ – the proportion between the viable heat boundary of the nanoparticle material, heat boundary of the liquid, g^* – increasing speed of gravity, β_T – coefficient of heat extension, and β_c – segregated Coefficient of development. What is significant

here is that $m = 0$ speaks to the current on the level plate and $m = 1$ speaks to the current at the stagnation point.

The following similarity variables can be used to non-linear Eqs. (1) – (6):

$$\begin{aligned} \xi &= \sqrt{\frac{(m+1)u_e(x)}{2\nu_f x}} y, \quad \psi = \sqrt{\frac{2\nu_f x u_e(x)}{m+1}} f(\xi) \\ \theta(\xi) &= \frac{T - T_\infty}{T_f - T_\infty}, \quad \varphi(\xi) = \frac{C - C_\infty}{C_f - C_\infty} \end{aligned} \quad (7)$$

Here $u_e(x)$ – potential stream speed on the wedge. The speed parts along with the boundary layer and typical are given by

$$\begin{aligned} u &= U_\infty x^m f'(\xi) \\ v &= -\sqrt{\frac{(m+1)U_\infty x^{m-1} \nu_f}{2}} \left[f(\xi) + \frac{m-1}{m+1} \xi f'(\xi) \right] \end{aligned} \quad (8)$$

Here $m = \frac{\beta}{2 - \beta}$ – wedge parameter, x – separation along the wedge surface, $u_e(x)$ – potential stream speed and $Re_x = \frac{xu_e(x)}{\nu_f}$ – Reynolds number. A stream work ψ is utilized rather than the potential capacity to naturally fulfill the Cauchy-Riemann conditions $u = \frac{\partial \psi}{\partial y}$ and $v = -\frac{\partial \psi}{\partial x}$ which prompts a decrease in the quantity of both ward factors and conditions. Concerning the boundary conditions and Eqs. (2)–(6) become:

$$\frac{\partial^3 f}{\partial \xi^3} + f \frac{\partial^2 f}{\partial \xi^2} - \frac{2m}{m+1} \left[1 - \left(\frac{\partial f}{\partial \xi} \right)^2 \right] + \frac{2\lambda}{m+1} (\theta + \delta\varphi) = 0 \quad (9)$$

$$\frac{\partial^2 \theta}{\partial \xi^2} + Pr \left[f \frac{\partial \theta}{\partial \xi} + Nb \frac{\partial \varphi}{\partial \xi} \frac{\partial \theta}{\partial \xi} + Nt \left(\frac{\partial \theta}{\partial \xi} \right)^2 \right] = 0 \quad (10)$$

$$\frac{\partial^2 \varphi}{\partial \xi^2} + Pr Le f \frac{\partial \varphi}{\partial \xi} + \frac{Nt}{Nb} \frac{\partial^2 \theta}{\partial \xi^2} = 0 \quad (11)$$

The transformed boundary conditions;

$$f(0) = 0, \frac{\partial f(0)}{\partial \xi} = 0, \frac{\theta(0)}{\partial \xi} = \sqrt{\frac{2}{m+1}} Nc [\theta(0) - 1], \quad (12)$$

$$\frac{\varphi(0)}{\partial \xi} = \sqrt{\frac{2}{m+1}} Nd [\varphi(0) - 1],$$

$$\frac{\partial f(\infty)}{\partial \xi} = 1, \theta(\infty) = 0, \varphi(\infty) = 0 \quad (13)$$

Characterize the connection between lightness and inertial power as indicated by the blended convection parameters as $\lambda = \frac{g^* \beta_T (T_f - T_\infty)}{\nu_f u_e^2(x)}$ and is used to describe the free,

forced, and mixed convection regimes. $\lambda \leq 1$ corresponds to pure forced convection, whereas $\lambda > 1$ corresponds to pure mixed convection, $\delta = \frac{\beta_C C_f - C_\infty}{\beta_T T_f - T_\infty}$ – buoyancy

parameter, $Pr = \frac{\nu_f}{\alpha_f}$ – Prandtl number for the nanofluid,

$Le = \frac{\alpha_f}{D_B}$ – Lewis number, $Nb = \tau D_B \frac{C_f - C_\infty}{\nu_f}$ – Brownian

motion parameter, $Nt = \frac{\tau D_T}{T_\infty} \frac{T_f - T_\infty}{\nu_f}$ – thermophoresis

parameter, $Nc = \frac{h_f}{k_f} \sqrt{\frac{\nu}{U_\infty}}$ – convective parameter, and

$Nd = \frac{h_{mass}}{k_f} \sqrt{\frac{\nu}{U_\infty}}$ – diffusion-convective parameter. Physical

amounts for reasonable purposes, the nearby Skin friction coefficient C_f , neighborhood Nusselt number Nu and neighborhood Sherwood number Sh which are characterized as:

$$C_f = \frac{2\mu}{\rho_f u_e^2} \left(\frac{\partial u}{\partial y} \right)_{y=0} \quad (14)$$

$$Nu = -\frac{x}{T_f - T_\infty} \left(\frac{\partial T}{\partial y} \right)_{y=0} \quad (15)$$

$$Sh = -\frac{x}{C_f - C_\infty} \left(\frac{\partial C}{\partial y} \right)_{y=0} \quad (16)$$

Using the similarity transformations as defined by (7) into (14)–(16), one can obtain

$$C_{fr} = C_f Re_x^{1/2} = \frac{2}{\sqrt{2-\beta}} f''(0) \quad (17)$$

$$Nu_r = Nu Re_x^{-1/2} = -\frac{1}{\sqrt{2-\beta}} \theta'(0) \quad (18)$$

$$Sh_r = Sh Re_x^{-1/2} = -\frac{1}{\sqrt{2-\beta}} \varphi''(0) \quad (19)$$

Here C_{fr} – reduced Skin friction, Nu_r – reduced Nusselt number, and Sh_r – reduced Sherwood number.

THE RUNGE-KUTTA-GILL METHOD

The non-linear differential conditions (9)–(11) subject as far as possible conditions (12)–(13) originate from the

third solicitation in f and the second solicitation in θ and ϕ . These conditions can be seen numerically utilizing a fourth solicitation Runge-Kutta-Gill technique that consolidates a terminating framework and Newton-Raphson innovation. We portray

$$f = Y_1, \frac{\partial f}{\partial \xi} = Y_2, \frac{\partial^2 f}{\partial \xi^2} = Y_3, \theta = Y_4, \frac{\partial \theta}{\partial \xi} = Y_5, \varphi = Y_6, \frac{\partial \varphi}{\partial \xi} = Y_7 \tag{20}$$

We also define the following:

$$\frac{\partial f}{\partial \xi} = F_1, \frac{\partial^2 f}{\partial \xi^2} = F_2, \frac{\partial^3 f}{\partial \xi^3} = F_3, \frac{\partial \theta}{\partial \xi} = F_4, \frac{\partial^2 \theta}{\partial \xi^2} = F_5, \frac{\partial \varphi}{\partial \xi} = F_6, \frac{\partial^2 \varphi}{\partial \xi^2} = F_7 \tag{21}$$

Substitute conditions (20) and (21) by conditions (9)–(11), these conditions are diminished to an arrangement of nine synchronous conditions of the principal request as follows:

$$F_1 = Y_2, \tag{22}$$

$$F_2 = Y_3, \tag{23}$$

$$F_3 = \left(\frac{2m}{m+1} \right) (1 - Y_2^2) - Y_1 Y_3 + \frac{2\lambda}{m+1} (Y_4 + \delta Y_6), \tag{24}$$

$$F_4 = Y_5, \tag{25}$$

$$F_5 = -\text{Pr}(Y_1 Y_5 + Nb Y_7 Y_5 + Nt Y_5^2), \tag{26}$$

$$F_6 = Y_7, \tag{27}$$

$$F_7 = -\text{Pr} Le (Y_1 Y_7) - \frac{Nt}{Nb} F_5, \tag{28}$$

The boundary conditions are given in (12) and (13) are replaced by

$$Y_1(0) = 0, Y_2(0) = 0, Y_3(0) = \sqrt{\frac{2}{m+1}} Nc (Y_4(0) - 1), \tag{29}$$

$$Y_7(0) = \sqrt{\frac{2}{m+1}} Nd (Y_6(0) - 1),$$

$$Y_2(\xi_\infty) = 1, Y_4(\xi_\infty) = 0, Y_6(\xi_\infty) = 0, \tag{30}$$

Here, ξ_∞ is selected as $\xi_\infty = 10$, depending on the set of the physical parameters.

The obscure introductory conditions are spoken to by $Y_3(0) = \zeta$, $Y_5(0) = t$ and $Y_7(0) = s$. We utilize the

Newton-Raphson technique to discover ζ , t and s with the goal that the arrangements of the conditions (22)–(28) fulfill as far as possible conditions (29)–(30). Right now, start with the underlying evaluations ($\zeta(0)$, $t(0)$, $s(0)$) through the trigger strategy. The Newton-Raphson calculation is stretched out to incorporate the halfway subordinates of the components of every factor. This will create the subordinates of $F(F_1, F_2, \dots, F_7)$ on ζ , t and s as follows:

$$F_\zeta(F_6, F_7, \dots, F_{10}), F_t(F_{11}, F_{12}, \dots, F_{15}), F_s(F_{16}, F_{17}, \dots, F_{20}), \tag{31}$$

Thus, we need to find $F_\zeta = 0, F_t = 0, F_s = 0$, simultaneously. Following Cebeci and Keller [32], these yields a system of algebraic equations which satisfy the boundary conditions when $\xi = 0$.

$$f'_\zeta \zeta + f'_t t + f'_s s + f' = 0, \theta'_\zeta \zeta + \theta'_t t + \theta'_s s + \theta = 0, \varphi'_\zeta \zeta + \varphi'_t t + \varphi'_s s + \varphi = 0 \tag{32}$$

Revamping the framework in condition (32) yields a grid condition;

$$Ax = B: \begin{bmatrix} f'_\zeta & f'_t & f'_s \\ \theta'_\zeta & \theta'_t & \theta'_s \\ \varphi'_\zeta & \varphi'_t & \varphi'_s \end{bmatrix} \begin{bmatrix} \zeta \\ t \\ s \end{bmatrix} = \begin{bmatrix} -f' \\ -\theta \\ -\varphi \end{bmatrix} \tag{33}$$

This lattice condition can be unraveled by Cramer’s standard. The following estimation of ζ , t and s can be computed by using the following formula:

$$\zeta^{(new)} = \zeta^{(old)} + \frac{\det(A_B(I, J))}{\det(A)}, \quad t^{(new)} = t^{(old)} + \frac{\det(A_B(I, J))}{\det(A)}, \quad s^{(new)} = s^{(old)} + \frac{\det(A_B(I, J))}{\det(A)} \tag{34}$$

When the estimations of ζ , t and s are known, we utilize the fourth-request Runge-Kutta-Gill strategy to tackle the main request of common differential conditions F_1, F_2, \dots, F_{20} . Following Gill [33], the Runge-Kutta recipe is

$$Y_{i+1} = Y_i + \frac{1}{6} h k_1 + \frac{1}{3} \left(\frac{2 - \sqrt{2}}{2} \right) h k_2 + \frac{1}{3} \left(\frac{2 + \sqrt{2}}{2} \right) h k_3 + \frac{1}{6} h k_4, \tag{35}$$

$$k_1 = F(Y_i) \tag{36}$$

$$k_2 = F \left(Y_i + \frac{h}{2} k_1 \right) \tag{37}$$

Table 1. The values of $f'(0)$ for various values of m when $\lambda = \delta = 0$

m	Rosenhead [34]	Watanabe [35]	Yih [36]	Yacob et al. [37]	Present result
0	1.232588	0.46960	0.469600	0.4696	0.469600
1/11		0.65498	0.654979	0.6550	0.654994
0.2		0.80213	0.802125	0.8021	0.802126
1/3		0.92765	0.927653	0.9277	0.927680
0.5			1.232588	1.0389	1.038903
1				1.2326	1.232588

$$k_3 = F \left(Y_i + \frac{1}{2}(-1 + \sqrt{2})k_1 + \left(1 - \frac{\sqrt{2}}{2}\right)k_2 \right) \quad (38)$$

$$k_3 = F \left(Y_i - \frac{\sqrt{2}}{2}k_2 + \left(1 + \frac{\sqrt{2}}{2}\right)k_3 \right) \quad (39)$$

Here h is signified as the progression size. In the present work, the progression size of $h = 0.01$ is seen as good in acquiring the numerical arrangements. For combination, the most extreme supreme relative contrast between two emphases is utilized inside a pre-doled out resilience $\epsilon < 10^{-6}$. If the distinction meets the combination criteria, the arrangement is expected to have merged and the iterative procedure is ended.

VALIDATION OF THE NUMERICAL PROCEDURE

To check the numerical program, the outcomes were contrasted and those recently announced in the writing. We thought about the particular qualities of the stream parameters with the investigation consequences of existing writing. These examinations are contrasted in Table 1 and Rosenhead [34], Watanabe [35], Yin [36], and Yacob et al. [37]. It is discovered that the examination is satisfactory and reliable with the current outcomes; any blunder can be viewed as trifling.

COMPUTATIONS AND DISCUSSION

The RK Gill technique is utilized to numerically comprehend the occasion fluctuating condition (9), the vitality condition (10), and the sort condition (11) under the boundary states of conditions (12) and (13). The count of the RK Gill technique was performed utilizing MATLAB. Different qualities of the parameters in question ie $A, \epsilon, M, \lambda, \delta, Nt, Nb, Pr,$ and Le have been numerically determined. The attributes of stream, heat and mass movements have been depicted and the outcomes have been accounted interns of designs and tables. In figs 2–19 the following data is generally utilized (unless otherwise stated): $Pr = 0.7, A = 0.2, M = 0.5, \lambda = 1, \delta = 0.5, Nt = 0.1, Nb = 0.1$ and $Le = 2$.

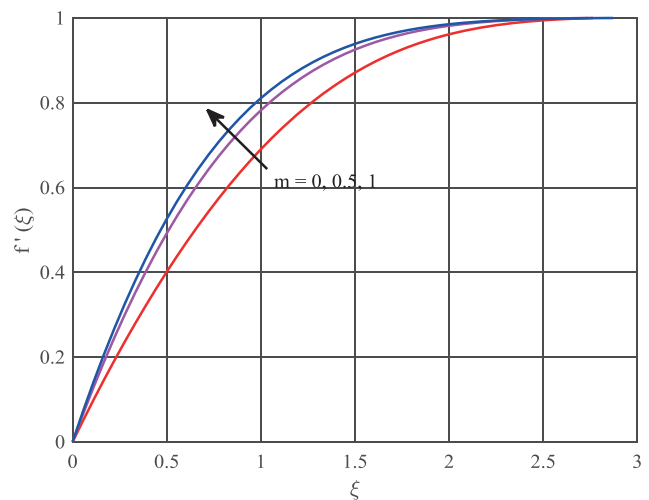


Figure 2. Velocity distribution $f'(\xi)$ for different values of m .

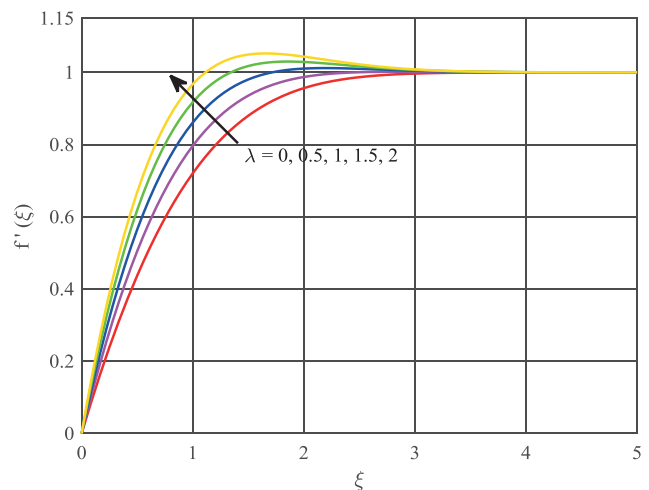


Figure 3. Velocity distribution $f'(\xi)$ for different values of λ .

The impact of the wedge parameter m on the dimensionless speed has appeared in Figure 2. It is seen that the dimensionless speed superficially increments with expanding wedge parameter m . Moreover, the thickness of the hydrodynamic boundary layer increments as the wedge parameter m increments. Figure 3 shows the impact of a

few qualities on the connection between the lightness and inertial powers as per the blended convection parameter λ in the dimensionless speed circulation. The figure shows that the dimensionless speed increments with the expansion of the blended convection parameter λ . The higher the estimation of λ , the more prominent the lightness impact in blended convection, and in this way, convection is quickened. Figure 4 shows the impact of wedge parameter m on the temperature of the nanofluid. It is seen that within the sight of a wedge-formed surface, the temperature of the nanofluid is lower contrasted with the temperature of a level surface. Physically, this reality can be delegated: for a level surface ($m = 0$), the dynamic or weight inclination to the liquid stream because of the temperature rise gets zero. Also, for wedge-molded surfaces, for instance ($m = 1$),

the intensity of liquid stream builds, which thusly quickens the current and moves more heat from the wedge-formed surface to the liquid. Thus, the temperature drops onto the surface. In Figure 5, the impact of the blended convection parameter λ has appeared on the nanofluid temperature. It is seen that as the estimation of the blended convection parameter λ expands, the temperature of the nanofluid and the thickness of the warm boundary layer decline. Figure 6 shows that the temperature of the nanofluid increments with the impact of the thermophoresis parameter Nt . This wonder depicts the way that thermophoresis powers because of temperature angles cause a fast stream away from the surface. Subsequently, additionally warming liquid streams out of the surface, so the temperature rises. Figure 7 shows the impact of the Brownian movement parameter Nb on the

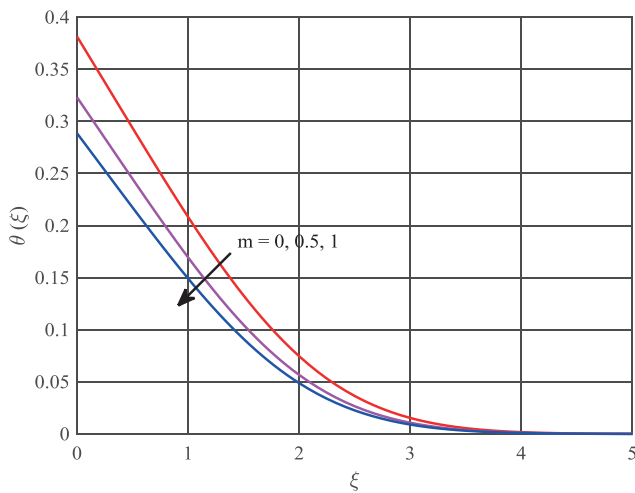


Figure 4. Temperature distribution $\theta(\xi)$ for different values of m .

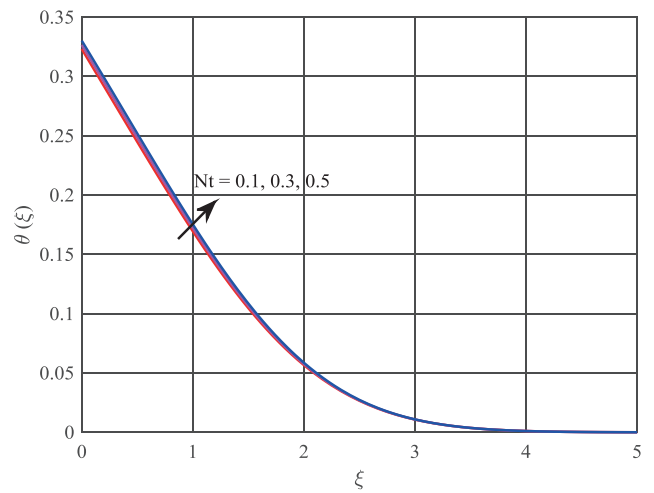


Figure 6. Temperature distribution $\theta(\xi)$ for different values of Nt .

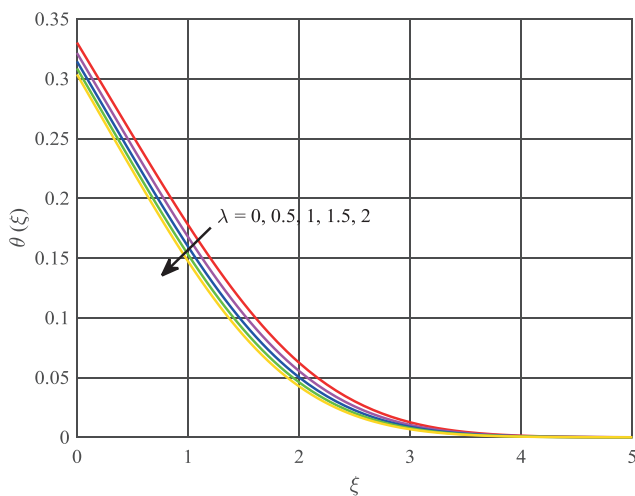


Figure 5. Temperature distribution $\theta(\xi)$ for different values of λ .

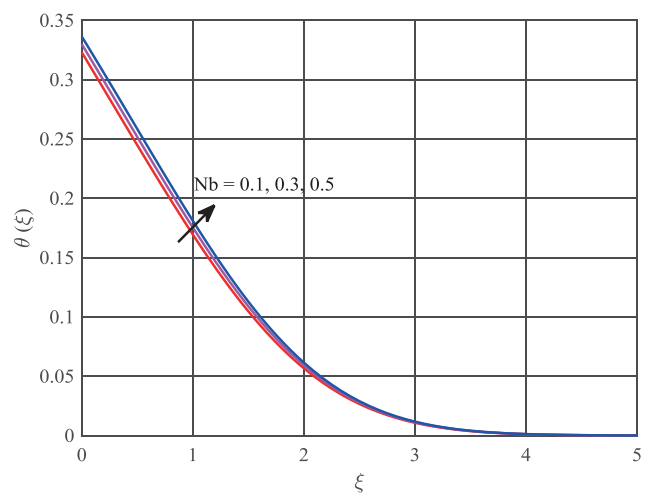


Figure 7. Temperature distribution $\theta(\xi)$ for different values of Nb .

temperature of the nanofluid. You can without much of a stretch find in the figure that as the Nb builds, the temperature of the nanofluid likewise increments. The temperature has a high incentive close to the boundary layer locale and diminishes step by step as the directions increment. This wonder can be deciphered as a constant estimation of Nb , which brings about an expansion in the Brownian speed of the nanoparticles and water atoms. Consequently the active vitality at the atomic level and nanoparticle level builds, which will convert into an expansion in nanofluid temperature. From the hypothesis of material science, we realize that $\frac{1}{2}mv^2 = \frac{3}{2}K_B \cdot T$, where K_B the Boltzmann's constant, T is the absolute temperature, and v is the velocity. It shows a steady connection between active vitality and temperature, which legitimizes the clarification given. An expansion in the quantity of Biot Nc compares to higher temperatures. As indicated by Figure 8, we break down that the temperature rises quickly from $Nc = 0.1$ to $Nc = 0.5, 1$, yet for temperatures more prominent than 1, the temperature rises gradually. It is obvious from the meaning of the Biot Nc number that the Biot Nc number speaks to the heat move coefficient h_f . For expanding the estimation of the Biot Nc number, the heat move coefficient builds, which produces heat, which thusly prompts an expansion in temperature. Figure 9 depicts that the temperature and thickness of the decreased warm boundary layer is the proportion of energy to warm diffusivity for littler Prandtl values. For countless Prandtl, the minute dissemination coefficient increments and the warm dispersion coefficient diminishes; for lower Prandtl liquids, the minute dispersion coefficient is lower than the warm dissemination coefficient. This more grounded warm diffusivity brings about a thicker warm boundary layer thickness. The impact of the wedge parameter m on the nanoparticle fixation is analyzed in Figure 10. It tends to be

seen that as the estimation of m builds, the grouping of the nanoparticles and the thickness of the important boundary layer decline. The impact of the blended convection parameter λ is inspected in Figure 11. It tends to be seen here that as the blending convection parameter λ expands, the fixation and thickness of the important boundary layer decline. Figures 12 and 13 show the adjustments in warm swimming and Brownian movement parameters at dimensionless focuses. It shows that within the sight of wedge-formed surfaces, the bend increments with the expansion of Nt esteem in the boundary layer district, and the contrary pattern is seen within the sight of Brownian movement parameters. In the figure alluding to Figures 14 and 15, it was seen that the convergence of the nanoparticles expanded for both convection and dispersion convection

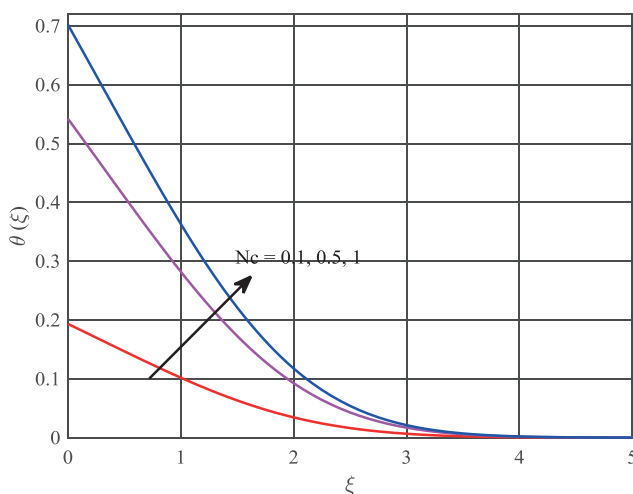


Figure 8. Temperature distribution $\theta(\xi)$ for different values of Nc .

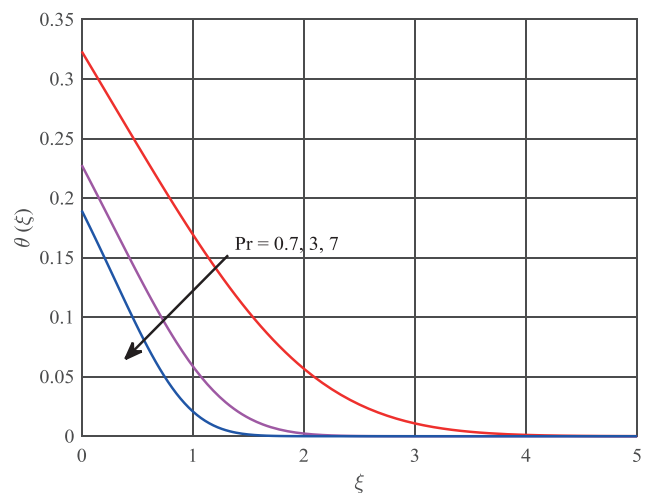


Figure 9. Temperature distribution $\theta(\xi)$ for different values of Pr .

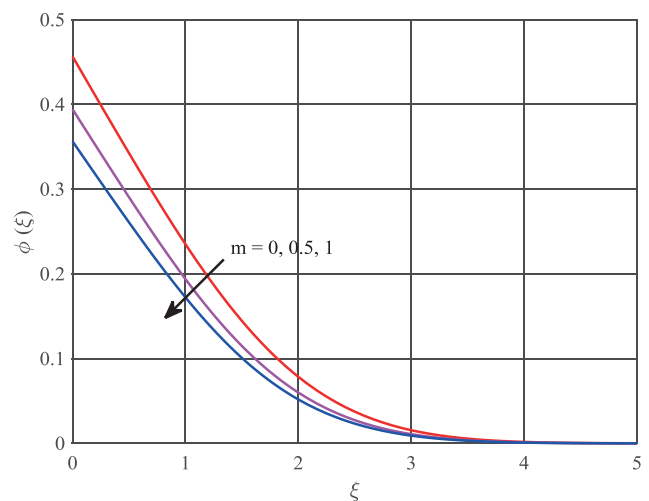


Figure 10. Concentration distribution $\phi(\xi)$ for different values of m .

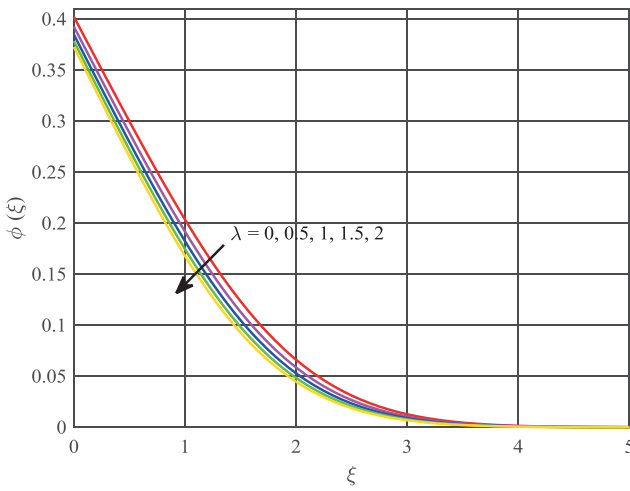


Figure 11. Concentration distribution $\phi(\xi)$ for different values of λ .

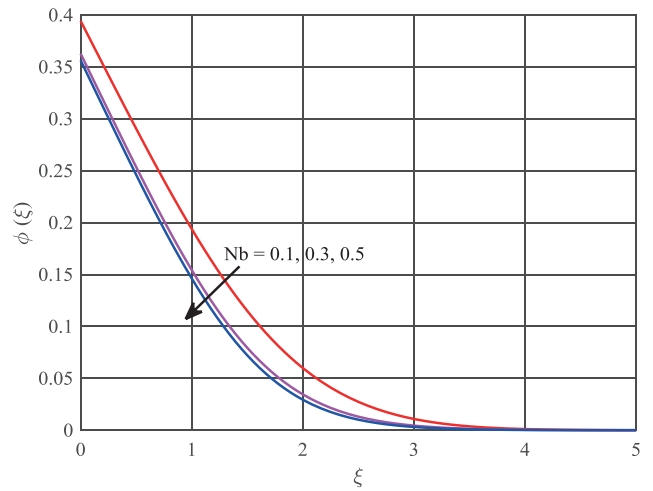


Figure 13. Concentration distribution $\phi(\xi)$ for different values of Nb .

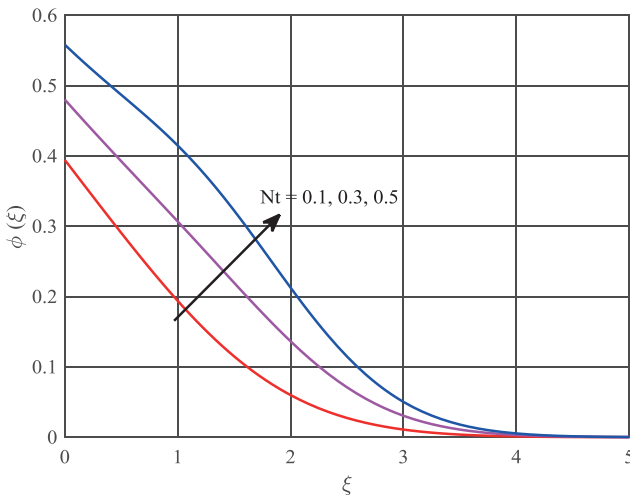


Figure 12. Concentration distribution $\phi(\xi)$ for different values of Nt .

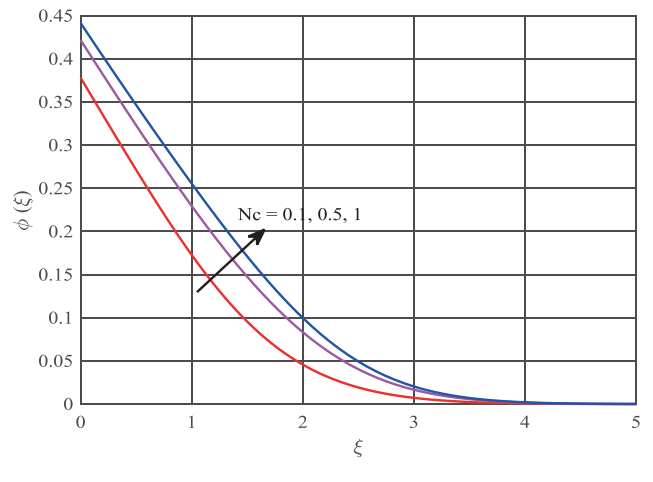


Figure 14. Concentration distribution $\phi(\xi)$ for different values of Nc .

parameters. In Figure 16, the concentration distributions of different values of the Lewis Le number are examined. Here, it tends to be seen that an expansion in the Lewis number demonstrates a fast abatement in focus. For various estimations of wedge parameters and blended convection parameters, the adjustments in skin erosion coefficient, heat move, and mass exchange rates are depicted in Figures 2 and 3, separately. As appeared in Figures 17, 18, and 19. As the estimation of the wedge parameter expands, the estimation of the skin grating coefficient increments, while the heat and mass exchange rates decline. Also, the higher the value of λ , the greater the buoyancy effect in mixed convection, thus accelerating the flow. Due to the large buoyancy effect λ , this leads to an increase in the effect of convective cooling. As λ quickens the speed of the liquid, the hot liquid

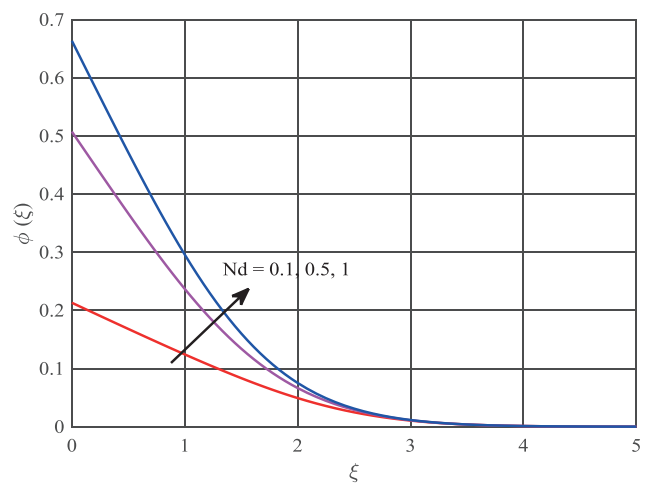


Figure 15. Concentration distribution $\phi(\xi)$ for different values of Nd .

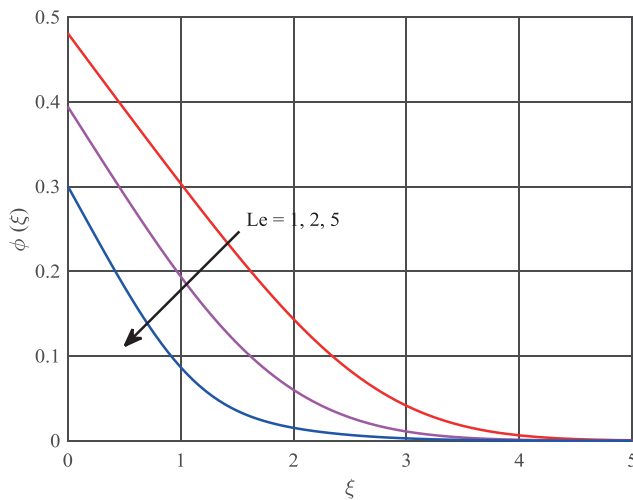


Figure 16. Concentration distribution $\phi(\xi)$ for different values of Le .

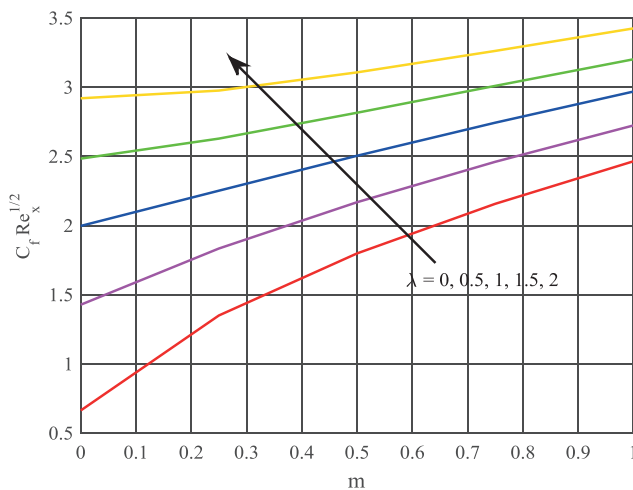


Figure 17. Skin friction coefficient $Re_x^{1/2} C_f$ for different values of λ for various m .

and high-fixation liquid close to the divider are supplanted by a lot of cooling liquid, so the heat and mass exchange rate increment. The Nusselt and Sherwood numbers of the liquid increment from unmodified convection (as $\lambda \rightarrow 0$) to unadulterated free convection ($\lambda > 1$). At long last, additionally to validate the present work, we compared the already available literature these qualities are determined in Table 1 (Rosenhead [34], Watanabe [35], Yih [36] and Yacob et al. [37]). The table checks the exactness of the present work, as they are extremely reliable with past outcomes in basic cases.

CONCLUSION

The impacts of convective heat and mass conditions on the blended convection of wedge-molded nanofluids were

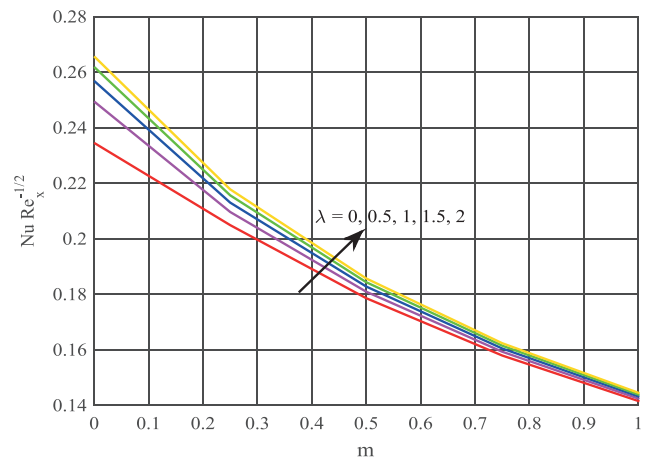


Figure 18. Nusselt number $Re_x^{-1/2} Nu$ for different values of λ for various m .

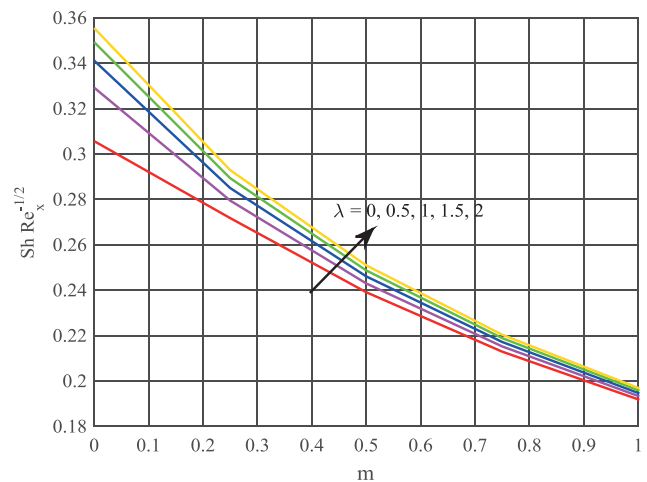


Figure 19. Sherwood number $Re_x^{-1/2} Sh$ for different values of λ for various m .

considered. The significant consequences of this investigation are as per the following:

1. Higher qualities of wedge parameters or the blended convection parameters can improve nanofluid speed and twisting minute constraining layer thickness.
2. The skin grinding coefficient is upgraded because of augmentation in the wedge parameter or blended convection parameter.
3. Temperature and concentration boundary layer thickness are expanding elements of the thermophoresis parameter or Brownian movement parameter or convective parameter.
4. The focus boundary layer thickness is more slender for higher estimations of the Brownian movement parameter or wedge parameter or blended convection parameter or Lewis number.

5. An increment in focus turns out to be progressively prevailing by expanding the estimations of the thermophoresis parameter in correlation with the dispersion – convective parameter.
6. Both heat and mass exchange rates are expanded because of augmentation in the blended convection parameter and it is the inverse for the wedge parameter.
7. The tale aftereffects of the present examination might be valuable for scholarly research in the field of heat and mass transfer, and industry.

REFERENCES

- [1] Falkner VM, Skan SW. Some approximate solution of the boundary layer equations. *Philos Mag* 1931;12:865–896. [\[CrossRef\]](#)
- [2] Hartree DR. On the equation occurring in Falkner and Skan's approximate treatment of the equations of boundary layer. *Proc Camb Philos Soc* 1937;33:223–239. [\[CrossRef\]](#)
- [3] Stewartson K. Further solution of Falkner and Skan equation. *Proc Camb Philos Soc* 1954;50:454–465. [\[CrossRef\]](#)
- [4] Hastings SP. Reversed flow solutions of Falkner and Skan equation. *SIAM J Appl Math* 1972;22:329–334. [\[CrossRef\]](#)
- [5] Botta EFF, Hut FJ, Veladman AEP. The role of periodic solution in Falkner and Skan for $\lambda \geq 0$. *J. Eng Math* 1986;20:81–83. [\[CrossRef\]](#)
- [6] Yih KA. Uniform suction/blowing on forced convection about a wedge: uniform heat flux. *Acta Mech* 1998;128:173–181.
- [7] Watanabe T. Thermal boundary layers over a wedge with uniform suction or injection in forced flow. *Acta Mech* 1990;83:119–126. [\[CrossRef\]](#)
- [8] Rajagopal, K.R Gupta AS Na TY. A note on Falkner and Skan flows of a non-Newtonian fluid. *Int J Nonlinear Mech* 1983;18:313–320. [\[CrossRef\]](#)
- [9] Zaturka MB, Banks WN A new solution branch of the Falkner and Skan equation. *Acta Mech* 2001;152:197–201. [\[CrossRef\]](#)
- [10] Na TY. *Computational Methods in Engineering Boundary Value Problems*. New York: Academic Press; 1979.
- [11] Asaithambi A. A finite difference method for the Falkner and Skan equation. *Appl Math Comput* 1998;92:135–141. [\[CrossRef\]](#)
- [12] Yacob NA, Ishak A, Pop I. Falkner and Skan problem for a static or moving wedge in nanofluids. *Int J Thermal Sci* 2011;50:133–139. [\[CrossRef\]](#)
- [13] Chamkha AJ, Mujtaba M, Quadri A, Issa C. Thermal radiation effects on MHD forced convection flow adjacent to a non-isothermal wedge in presence of a heat source and sink. *Heat Mass Transf* 2003;39:305–312. [\[CrossRef\]](#)
- [14] Gorla RSR, Chamkha AJ, Rashad AM. Mixed convective boundary layer flow over a vertical wedge embedded in a porous medium saturated with a nanofluid natural convection dominated regime. *Nanoscale Res Lett* 2011;6:1–9. [\[CrossRef\]](#)
- [15] Khan WA, Pop I. Boundary layer flow past a wedge moving in a nanofluid. *Math Prob Eng* 2013;2013:637285. [\[CrossRef\]](#)
- [16] Kasamani RM, Muhaimin I, Kandasamy R. Laminar boundary layer flow of a nanofluid along a wedge in presence of suction/ injection. *J Appl Mech Tech Phys* 2013;54:377–384. [\[CrossRef\]](#)
- [17] Kandasamy R, Muhaimin I, Khamis AB, bin Roslan R. Unsteady Hiemenz flow of Cu–water nanofluid over a porous wedge in presence of thermal stratification due to solar energy radiation. *Int J Thermal Sci* 2012;65:196–205. [\[CrossRef\]](#)
- [18] Das K, Acharya N, Prabir Kumar K. Influence of variable fluid properties on nanofluid flow over a wedge with surface slip. *Arab J Sci Eng* 2018;43:2119–2131. [\[CrossRef\]](#)
- [19] Gangadhar K, Kannan T, Sakthivel G, Dasaradha Ramaiah K. Unsteady free convective boundary layer flow of a nanofluid past a stretching surface using a spectral relaxation method. *Int J Ambient Energy* 2018;41:609–616. [\[CrossRef\]](#)
- [20] Gangadhar K, Keziya K, Ibrahim SM. Effect of thermal radiation on engine oil nanofluid flow over a permeable wedge under convective heating: Keller box method. *Multidiscip Model Mater Struct* 2018;15:187–205. [\[CrossRef\]](#)
- [21] Hiemenz Kç Die Grenzschicht an einem in den gleichförmigen Flüssigkeitsstrom eingetauchten geraden Kreiszyylinder. *Dinglers Polytech J* 1911;326:321–324. (Deutsch)
- [22] Stuart JT. The viscous flow near a stagnation-point when the external flow has uniform vorticity. *J Aerosp Sci* 1959;26:124–125. [\[CrossRef\]](#)
- [23] Chiam TC. Stagnation-point flow towards a stretching plate. *J Phys Soc Jpn* 1994;63:2443–2444. [\[CrossRef\]](#)
- [24] Wang CY. Stagnation flow towards a shrinking sheet. *Int J Nonlinear Mech* 2008;43:377–382. [\[CrossRef\]](#)
- [25] Verdunstung FN. Wärmeübertragung und Geschwindigkeitsverteilung bei zweidimensionaler und rotations symmetrischer laminarer Grenzschicht-stromung. *Lunds Univ Arsskr NF Avd* 1940;2:35. (Deutsch) [\[CrossRef\]](#)
- [26] Homann F. Der Einfluss grosser Zähigkeit bei der Stromung um den Zylinder und um die Kugel. *Z Angew Math Mech* 1936;16:153–164. (Deutsch) [\[CrossRef\]](#)
- [27] Howarth L. The boundary layer in three-dimensional flow. Part II: the flow near a stagnation-point. *Philos Mag VII* 1951;42:1433–1440. [\[CrossRef\]](#)

- [28] Davey A. Boundary layer flow at a saddle point of attachment. *J Fluid Mech* 1961;10:593–610. [\[CrossRef\]](#)
- [29] Labropulu F, Xu X, Chinichian M. Unsteady stagnation point flow of a non-Newtonian second grade fluid. *Int J Math Math Sci* 2003;60:3797–3807. [\[CrossRef\]](#)
- [30] Sandeep N, Sulochana C, Isaclare A. Stagnation-point flow of a Jeffrey nanofluid over a stretching surface with induced magnetic field and chemical reaction. *Int J Eng Res Afr* 2016;20:93–111. [\[CrossRef\]](#)
- [31] Mahmood K, Noveel Sadiq M, Sajid M, Nasir A. Heat transfer in stagnation point flow of a Jeffrey fluid past a lubricated surface. *J Brazil Soc Mech Sci Eng* 2019;41:65. [\[CrossRef\]](#)
- [32] Cebici T, Keller H. Shooting and parallel shooting methods for solving the Falkner–Skan boundary-layer equation. *J Comput Phys* 1971;7:289–300. [\[CrossRef\]](#)
- [33] Gill S. A process for the step-by-step integration of differential equations in an automatic digital computing machine. *Math Proc Camb Philos Soc* 1951;47:96–108. [\[CrossRef\]](#)
- [34] Rosenhead, L. *Laminar Boundary Layer*. Oxford: Oxford University Press; 1963. [\[CrossRef\]](#)
- [35] Watanabe T. Thermal boundary layers over a wedge with uniform suction or injection in forced flow. *Acta Mech* 1990;83:119–126. [\[CrossRef\]](#)
- [36] Yih KA. Uniform suction/blowing effect on forced convection about a wedge: uniform heat flux. *Acta Mech* 1998;128:173–181. [\[CrossRef\]](#)
- [37] Yacob NA, Ishak A, Pop I. Falkner Skan problem for a static or moving wedge in nanofluids. *Int J Therm Sci* 2011;50:133–139. [\[CrossRef\]](#)
- [38] Regue HM, Bouali B, Benchatti T, Benchatti A. Analysis and simulation of thermal performance of a PTC with secondary reflector. *J Therm Eng* 2021;7:1531–1540. [\[CrossRef\]](#)
- [39] Gaur MK, Tiwari GN, Singh P, Kushwah A. Heat transfer analysis of hybrid active solar still with water flowing over glass cover. *J Therm Eng* 2021;7:1329–1343. [\[CrossRef\]](#)
- [40] Madderla S, Ramasamy D, Sudhakar K, Kadirgama K, Wan Harun Ws. Heat transfer performance of a radiator with and without louvered strip by using Graphene-based nanofluids. *J Therm Eng* 2021;7:1315–1328. [\[CrossRef\]](#)
- [41] Akcay S, Akdag U. Mixed convection heat transfer from a vertical flat plate subjected to periodic oscillations. *J Therm Eng* 2021;7:1377–1391. [\[CrossRef\]](#)